

ORIGINAL RESEARCH

Active noise control by means of high frequency injection in electric motors

 Stefanos Skoulaxinos  | Pat Wheeler | Gaurang Vakil

Power Electronics, Machines and Control (PEMC) Group, University of Nottingham, Nottingham, UK

Correspondence
 Stefanos Skoulaxinos.
Email: Stefanos.Skoulaxinos@nottingham.ac.uk
Funding information

Clean Sky 2 European Union's Horizon research and innovation programme, Grant/Award Number: 831877

Abstract

Machine acoustics is an important area of research impacting the quality and comfort of human life. With increased levels of electrification and the wider use of electric motors, the contribution of motor drives towards quieter acoustic systems becomes increasingly important. This paper presents a novel acoustic improvement method involving the use of acoustic waves generated from High Frequency Injection to perform Active Noise Control. Although High Frequency Injection has been used widely in the domain of sensorless motor control, its acoustic generation process has been so far perceived as a negative by-product. This paper presents the analysis and experimental results from the application of the proposed method to the Helicopter Electro-Mechanical Actuation System. Considering the extensive use of motor drives in a number of industries, the proposed practice of High Frequency Injection Active Noise Control can have a significant impact to future applications.

KEYWORDS

AC motors, acoustic noise, aerospace components

1 | INTRODUCTION

The method of active noise control (ANC) was first introduced by a German physicist and inventor, Paul Lueg in 1936 [1]. The application proposed by Lueg [1] involved cancelling sinusoidal acoustic noise by means of introducing an inverted-polarity sound wave using a speaker. In the 1950s and 1960s, ANC was advanced further by Lawrence J. Fogel, introducing a number of noise cancelling (NC) headphone applications for helicopter and aircraft cockpits [2]. The designs proposed by Fogel [2] aimed to improve the communication between the pilots within a cockpit and reduce the acoustic noise they are exposed to. With the technological advancement of digital signal processing (DSP) systems, the method of ANC became easier to commercialise, leading to publicly available NC headphones in the 1980s.

In the subsequent decades, intensive research and development has taken place in the area of ANC by Academia and Industry. In the aerospace sector, Ultra commercialised state-of-the-art ANC systems were used for a number of turbo-

propeller aircrafts (Bombardier, Lockheed Martin, Beechcraft King Air, and Saab) [3, 4]. The above ANC applications by Ultra involve the installation of microphones, speakers, and vibratory devices within the cabin of aircrafts to reduce the acoustic noise experienced by the passengers.

The marine and submarine transport sectors have been another active area of ANC. The acoustic stealthiness of submarines and military vessels is essential for the safety of the crew enabling them to carry out their defence activities. The collaboration between the University of Sheffield and BAE Systems [5, 6] as well as the research performed by the University of Adelaide [7] are two examples of active noise/vibration control in submarine applications. Other research efforts in marine ANC include [8] suppressing vibrations from a marine diesel generator [9, 10], involving the use of piezoelectric actuators [11], and controlling the rotation of masses connected to a motor drive. In each of the above methods, vibratory devices are installed in the application that produce anti-phase counteracting vibrations against a primary noise source to be cancelled.

This is an open access article under the terms of the [Creative Commons Attribution](https://creativecommons.org/licenses/by/4.0/) License, which permits use, distribution and reproduction in any medium, provided the original work is properly cited.

© 2024 The Authors. *IET Electric Power Applications* published by John Wiley & Sons Ltd on behalf of The Institution of Engineering and Technology.

A similar trend exists in the automotive and rail transport sectors. Silentium [12] provides integrated solutions performing ANC for land vehicles and trains. Their designs involve the installation of microphones and loudspeaker arrays performing noise cancellation [12].

One additional topic of research in the area of ANC involves a key implementation algorithm named least mean square (LMS). A closed-loop ANC system typically samples the primary noise to be cancelled using what is known in the research area as a reference microphone producing signal $x(n)$ as shown in Figure 1a. A second microphone named error microphone is placed at the noise cancellation point-of-interest producing signal $e(n)$. An adaptive filter is then used in conjunction with a least mean square (LMS) implementation to calculate the anti-noise signal $y(n)$ that is fed to a speaker. The purpose of the LMS algorithm is to continuously adjust the weight of the adaptive filter's gains and therefore align the frequency and signal characteristics of the anti-noise $y(n)$ to that of the primary noise $x(n)$. Upon each LMS calculation iteration, the weights of the adaptive filter's gains are updated as per the following equation:

$$w(n+1) = w(n) - \mu x(n)e(n) \quad (1)$$

where $w(n)$ is the weights of the adaptive filter, μ is the learning step of the LMS algorithm, $x(n)$ is the reference microphone noise signal, and $e(n)$ is the signal from the error microphone.

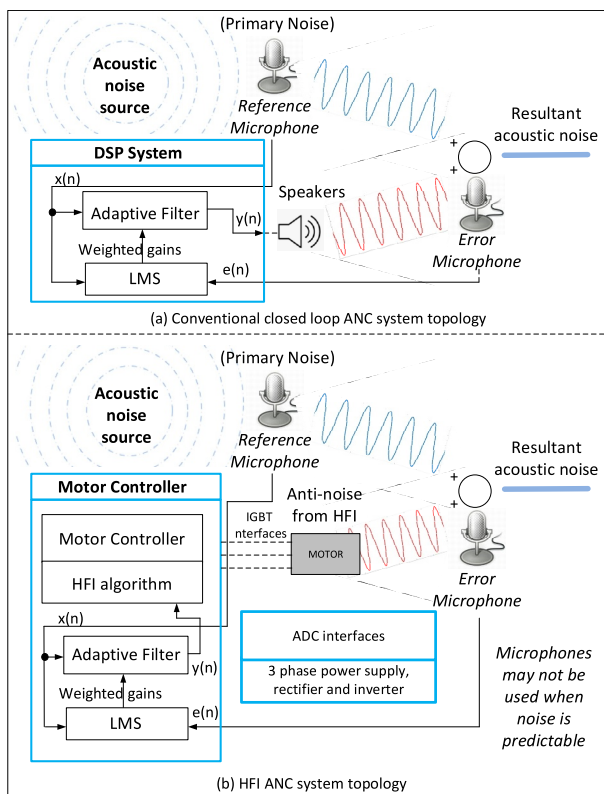


FIGURE 1 HFI ANC system diagram. (a) Conventional ANC topology, (b) Proposed HFI ANC system topology. ANC, active noise control; HFI, high frequency injection.

The LMS algorithm and its variants provide an efficient implementation for the calculation process of the anti-noise $y(n)$. A number of LMS variants have thus been proposed such as the Filtered-x LMS, Block LMS, Ajoint LMS, and others [13–15].

Active noise control has advanced in the past decades in a number of industries. One motivation for this interest is that passive acoustic methods tend to reduce but not eliminate acoustic noise. Ear defenders for instance can only attenuate the amplitude of the noise reaching a human's ears. Additionally, passive insulative strategies at industrial scale usually add more weight to the target application [16] relative to active control methods. ANC methods are thus useful providing one additional defence layer against acoustic noise and are generally applied in conjunction with passive insulative methods.

The novel idea proposed in this paper is utilising the mechanical infrastructure of a motor drive as an acoustic generator to achieve ANC. Past research in the area of ANC involves the installation of vibratory devices such as speakers. In contrast, the research presented in this paper re-uses the electrical and mechanical infrastructure used for the spinning of a motor to achieve ANC. The method therefore adds an acoustic generation capability to an otherwise conventional motor drive. To achieve this acoustic capability, a method that has been used so far for other purposes is deployed. High frequency injection (HFI) has been used over the past 30 years in the area of sensorless motor control. It involves superimposing a high frequency (HF) voltage to a salient motor to identify its rotor angle. One so far identified as a drawback of this method is the generated acoustic noise. The studies of [17, 18] have attempted to suppress and reduce the perception of this noise. The research presented in this paper attempts to harness the vibratory acoustic energy produced by HFI to achieve ANC.

The hardware platform selected to demonstrate that the proposed concept is an electric actuator controlling the swash plate of a helicopter, namely the Helicopter Electro-Mechanical Actuation System (HEMAS). The proposed method, however, could be applied to any type of motor drive and electrical machine.

This paper begins by providing a theoretical background on HFI and Acoustics. This theoretical background is vital to understand how the method of HF injection introduces vibrations that turn into acoustic noise. It then continues with a description of the proposed HFI ANC method and finally presents modelling and experimental results, when the scheme is applied to the HEMAS motor drive.

2 | HIGH FREQUENCY INJECTION AND ACOUSTICS

2.1 | High Frequency Injection

High frequency (HF) injection has been used over the past 30 years for a wide range of motor types including permanent magnet synchronous motors (PMSMs) [19–21], switched

reluctance motors (SRMs) [22], brushless DC motors (BLDCs) [23], and induction motors [24]. This family of sensorless algorithms takes advantage of the saliency of an electrical machine to identify the angle of its rotor. A motor is classified as salient if the magnetic field of its rotor is characterised by projecting poles. The saliency of a motor results in its phase inductance to vary as a function of the rotor angle. By injecting a HF voltage across the phases of a salient machine, the amplitude of the resultant HF currents can thus be used to identify the phase inductance and the rotor angle.

A key equation that forms the basis of saliency methods defining the relation between voltage injection and phase current is shown below and is derived from Faraday's law:

$$V = L \frac{dI}{dt} \quad (2)$$

There is a rich variety of HFI techniques depending on the axis that the injection is applied to stationary or synchronous frames [21, 25], the injection voltage shape (sinusoidal or square) [26], the injection frequency [17], and demodulation algorithm variations [17, 22, 23, 26]. Although HF injection methods provide a practical solution towards rotor angle estimation, one known drawback is that the generated HF currents create torque pulsations that in turn produce acoustic noise [17, 18, 27]. The research presented in this paper proposes to use the generated acoustic noise from HFI to achieve ANC.

2.2 | Acoustics

Fundamentals of Acoustics: Acoustics is a branch of physics, and it is naturally divided into four areas [28]:

- The mechanism of sound generation, that is, the phenomenon initiated by the vibration of an object within an elastic medium.
- The propagation of this vibratory energy through an elastic medium in the form of sound waves. The molecules of a medium can be perceived in the context of acoustics as particles interconnected by springs (bonds between molecules). The initially vibrating object initiates vibration of the molecules surrounding it, which in turn transfer this vibration into other surrounding molecules causing a wave of varying pressure/compression travelling through an elastic medium until the energy is dissipated. The medium through which sound propagates can be a gas, a liquid, or a solid object.
- The physical reception of this vibratory energy (variation of pressure) from a receiver using an ear or a microphone.
- The psychological perception of noise, that is, whether a sound is perceived as pleasant or not by the receiver.

Each of the above areas is of interest with regard to this research. The acoustic generation process initiated by the

motor's vibration due to HFI, the propagation of this noise, its interaction with a primary noise, and the resultant acoustic suppression process are all relevant to the proposed method and analysed in this paper.

Acoustics from HFI: The HF voltages applied to the phases of a motor create HF currents that produce torque pulsations and vibrations within the motor and its connected mechanical infrastructure. This vibratory energy on the motor drive initiates vibration of the surrounding air molecules creating a travelling sound wave perceived by a receiving ear or microphone.

To characterise the acoustic noise generated from HFI in more detail, it is necessary to revisit the equivalent mathematical model of the motor of interest. In the case of the HEMAS platform, the equivalent circuit model of a PMSM in the synchronous frame is shown in the following equation:

$$\begin{bmatrix} V_d \\ V_q \end{bmatrix} = \begin{bmatrix} R_s i_d + \frac{d}{dt}(L_d i_d + \Psi_f) - \omega_r L_q i_q \\ R_s i_q + \frac{d}{dt}L_q i_q + \omega_r(L_d i_d + \Psi_f) \end{bmatrix} \quad (3)$$

where V_d and V_q are stator voltages in the synchronous frame, R_s is the stator resistance, i_d and i_q are stator currents in d and q axis, ω_r is the rotor's electrical angular speed, L_d is the d axis inductance, L_q is the q axis inductance, and Ψ_f is the rotor flux.

Assuming the HFI method is applied to the estimated d axis—a method that is commonly used in PMSMs [20, 21]—then a portion of the HF voltage is deposited to the d axis and the remaining portion to the q axis as per Equations (4) and (5) below:

$$V_{d-HF} = V_{\text{carrier}} * (\cos \omega_c t) * \cos \theta_{\text{err}} \quad (4)$$

$$V_{q-HF} = V_{\text{carrier}} * (\cos \omega_c t) * \sin \theta_{\text{err}} \quad (5)$$

Assuming that the voltage drop due to the motor's resistance $R_s i_d$ and $R_s i_q$ and due to the Back Electro Motive Force is negligible relative to the voltage drop due to the motor's inductance, Equation (3) becomes

$$\begin{bmatrix} V_{d-HF} \\ V_{q-HF} \end{bmatrix} = \begin{bmatrix} V_{\text{carrier}} * (\cos \omega_c t) * \cos \theta_{\text{err}} \\ V_{\text{carrier}} * (\cos \omega_c t) * \sin \theta_{\text{err}} \end{bmatrix} \approx \begin{bmatrix} L_d \frac{d}{dt}(i_d) \\ L_q * \frac{d}{dt}i_q \end{bmatrix} \quad (6)$$

Based on Equations (4), (5), and (6), a sinusoidal HF voltage V_{d-HF} and V_{q-HF} applied to the d and q axis, will create sinusoidal currents of the same frequency in the two synchronous axis frames. To calculate the resultant torque from these HF currents, the formula for a PMSM is given below:

$$T_{\text{PMSM}} = (3/2) * (P/2) * (\lambda_m * I_q + (L_d - L_q) * i_d * i_q) \quad (7)$$

where P is the number of poles, λ_m is the flux linkage, L_d and L_q is the d and q axis motor inductance, and i_d and i_q are the d and q axis motor current.

Considering Equations (6) and (7), when a HF voltage of n kHz is applied to a PMSM, the resultant HF currents (i_d and i_q) and torque pulsations experienced by the motor are also centred at the same frequency. As the motor's mechanical structure vibrates due to HFI, it initiates the vibration of its surrounding air molecules at this frequency. This vibration of the air molecules at n kHz travelling in the air is what is perceived as acoustic noise centred at this frequency. The claim on this correlation between the frequency of HFI and the frequency of the generated acoustic noise is validated experimentally in Section 5 of this paper.

Simple Harmonic Motion modelling: To appreciate the propagation and interaction of acoustic waves in an elastic medium, it is useful to consider the model of a Simple Harmonic Motion (SHM) system as shown in Figure 2. Consider a spring is attached on one end of a stationary position and an object of mass m is attached on the other end. Assume the object is oscillating around an equilibrium point based on the equation of linear displacement x :

$$x = A * \sin \omega t \quad (8)$$

where x is the displacement from the point of equilibrium, A is the amplitude of the oscillation, and $\sin \omega t$ expresses the frequency of this vibratory movement.

Using Newton's second law of motion, the force that produces this motion is:

$$F = -m * A * \omega^2 * \sin \omega t \quad (9)$$

As a result of Equation (9), when the object is displaced towards the right, there is a force attempting to restore it to the equilibrium point towards the left and so on initiating an oscillation of the object around the equilibrium point. When an elastic body, such as a gas, a liquid, or solid, is subjected to

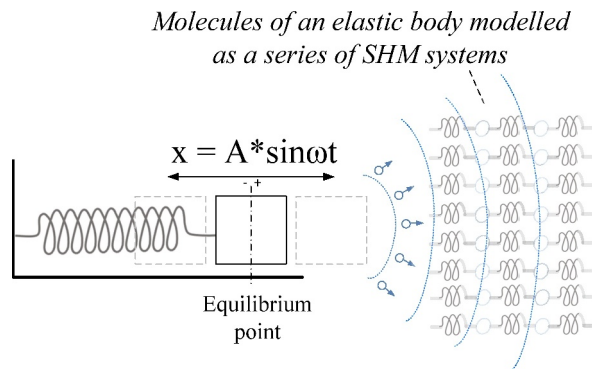


FIGURE 2 Analysis based on simple harmonic motion.

strain in the form of vibration or displacement, it can be shown [28] that the molecules of this body exhibit the behaviour of a series of SHM systems (See Figure 2).

In the context of Acoustics and under the proposed HFI ANC method, the motor's mechanical infrastructure oscillating at n kHz due to HFI can be seen as the stationary spring of Figure 2. The vibration of the motor being in direct contact with air initiates the displacement and vibration of the immediately surrounding air molecules. The motion of these air molecules exhibits the same characteristics of the motion of the original source [28] as shown in Equation (8). Considering the spring-like interconnection of an elastic medium, the initially vibrating air molecules transfer their movement to their surrounding molecules creating a wave of travelling condensations and rarefactions [28]. This vibratory energy travels through the air at the speed of sound. Based on the SHM modelling method [28], the spring-like behaviour of the medium's particle interconnections enforces the motion of the medium molecules to follow the motion of the initially vibrating object with a phase retardation associated with the speed of sound.

The above modelling method of SHM can also be used to understand the ANC process. When the travelling vibratory energy from two noise sources arrives at a point-of-interest, if this oscillatory movement from the two waves is synchronised and in-phase, the air molecules at this point will be subjected to an additive vectorial force. The increased force will initiate the air molecules behaving as an SHM model to oscillate with higher displacement, causing increased vibration and a louder acoustic noise. If on the other hand, the two waves are in anti-phase, the force from the two travelling waves will oppose each other restraining the molecules of the point-of-interest from vibration and reducing acoustic noise.

Fluid dynamics and acoustic modelling: The mechanism of sound generation and propagation in an elastic medium relates to this medium behaving as a fluid [29, 30]. A number of modelling methods in the scientific area of fluid dynamics are thus commonly used to analyse Acoustics. The Navier–Stokes Equations (10), (11) that govern Fluid Dynamics are thus fundamental in complex Acoustics analyses [29]:

$$\frac{\partial \rho}{\partial t} + \frac{\partial \rho v_i}{\partial x_i} = 0 \quad (10)$$

$$\frac{\partial v_i}{\partial t} + v_j \frac{\partial v_i}{\partial x_j} = \frac{1}{\rho} \frac{\partial \tau_{ij}}{\partial x_j} + B_i \quad (11)$$

where ρ is the density of the fluid, t is time, v_i is the total velocity of the fluid in the i th direction, x_i is the direction of the component, τ_{ij} is the stress component, and B_i is the body force that is applied to the fluid (e.g. gravity). The above Navier–Stoke equations are essentially based on the Newton's second law applied to fluids, that is, the acceleration of a mass of fluid is proportional to the force applied to it.

Due to the non-linear nature of Navier–Stoke equations and their associated complexity, simplified versions of these

equations are more commonly encountered in Acoustics including the “Reynolds-Averaged Navier–Stokes” (RANS), large eddy simulation (LES), and direct numerical simulation (DNS) [31–33].

Another type of fluid dynamics equations that can be encountered is the linearised Euler equations (LEE) [29] that are closely related to the Navier–Stokes equations mentioned above but do not take into account the fluid viscosity.

Acoustic analysis for some applications can be simplified using tools such as Matlab and not necessarily needing to apply fluid dynamic equations. The acoustic analysis presented in this paper uses Matlab and Matlab's k -wave, simulating how waves interact in the elastic medium with these results being validated in the hardware testing section.

Geometric spreading of sound waves and losses: A widely used strategy for the analysis of geometric sound propagation involves the assumption of a point source where the sound is considered to be born and then a spherical expansion of this vibratory energy takes place within a homogeneous medium in the three-dimensional space [34, 35]. The sound intensity on each direction based on this acoustic model and assuming a lossless propagation is governed by the following equation:

$$I = \frac{P}{4\pi r^2} \quad (12)$$

where $I[W^{-2}]$ is the sound intensity at a distance or r metres from the point source of Power $P[W]$.

The sound attenuation expressed in Equation (12) can be appreciated considering that as the sound propagates in three-dimensional space, the initial energy is divided to all directions in a spherical manner.

Represented in logarithmic scale, sound pressure can be expressed in the equation below also known as the inverse square law for point sources [34]:

$$L_p = L_W - 20 \log(r) - 11 \text{ dB} \quad (13)$$

where L_p is the sound pressure located at distance r from the point source versus the power at the source L_W . Based on Equation (13), the sound pressure reduces by 6 dB as the distance from the source doubles [34, 36].

While Equations (12) and (13) hold for cases where the acoustic noise expands equally on all directions in a spherical manner, many acoustic sources have a tendency to direct the majority of their vibratory energy on one direction. Consider for instance a speaker or a human's voice which will produce sound that is more audible for observers located at the front of them. Equation (13) is therefore re-written as per ref. [34]:

$$L_p = L_W + DI - 20 \log(r) - 11 \text{ dB} \quad (14)$$

where L_p is the sound pressure located at distance r from the point source versus the power at the source L_W and directivity index is the DI. The DI in Equation (14) is a variable defining how directed is the sound emission in the three-dimensional

space. With sound being directed on one direction as per Equation (14), the intensity does not disperse on all directions and can remain higher on the direction of interest.

While Equations (12) to (14) define how the vibratory sound energy is expanded in space in a lossless medium, in practice, a part of the travelling vibratory energy will be dissipated in the atmosphere in the form of heat as it travels through the air [34], a phenomenon also known as atmospheric absorption. The cause of this lossy attenuation of sound is due to heat conduction, shear viscosity, and molecular relaxation issues [37]. The formula that governs atmospheric absorption is given below:

$$p = p_0 e^{-ax/2} \quad (15)$$

where p is the sound pressure at distance x from a position where the pressure is p_0 and a is the absorption coefficient for a given elastic medium dependent on humidity temperature and pressure [34].

In the case of the research presented in this paper, the acoustic waves from HFI are modelled to propagate uniformly in the three-dimensional space excluding atmospheric losses. Despite this simplification in the modelling process, the simulation results are supported and validated by the hardware testing section.

Effect of reflections and wind: Other than the sound attenuation due to geometric propagation and atmospheric absorption, the complexity of sound propagation increases further when the acoustic waves interact with their surrounding objects or when exposed to wind [29, 34, 38]. Sound waves can bounce and change direction and characteristics when interacting with their surrounding objects. This interaction results in the originally travelling wave to change many of its characteristics.

Reflections in the laboratory where the HFI ANC was applied to the HEMAS platform were not considered in simulations; however, this simplified acoustic modelling was validated and supported by means of hardware testing.

This section of the paper attempted to provide an analytical background of sound generation and propagation. The proposed method of ANC by means of HF injection will be introduced, simulated, and tested in subsequent sections.

3 | CONVENTIONAL ANC METHODS

ANC is the method of introducing an acoustic waveform, termed anti-noise, that is in anti-phase relation to an existing primary noise source within a system. The two waves, primary noise and anti-noise, interact in the medium cancelling each other out resulting in a quieter acoustic system (See Figure 1a). An ANC system would typically be composed of a set of microphones capturing the existing noise, a DSP system analysing the captured sound and a speaker producing anti-noise.

One disadvantage of the conventional topology of the above-mentioned ANC systems involves the installation of

microphones, speakers, and vibration-generating devices. The proposed HFI ANC method does not necessitate the installation of speakers and attempts instead to utilise the existing mechanical infrastructure of a motor drive instead.

4 | THE HFI ANC METHOD

4.1 | The proposed method

The HFI ANC method proposed in this paper involves superimposing a HF voltage and controlling its frequency and phase so as to be in anti-phase relation and cancel an existing noise source within a system (See Figure 3, Figure 1b, Figure 4).

There are cases where the residing acoustic noise to be cancelled has a predictable pattern and the ANC can be applied in an open loop manner [39]. An example of such a predictable noise is that from an electric compressor that experiences load and acoustic pulses at predefined mechanical angle. In such cases, the HFI ANC method can be applied without the need of a microphone using a feed forward open-loop method. In cases that the acoustic noise is more random in nature, the HFI ANC method is best applied in conjunction with a

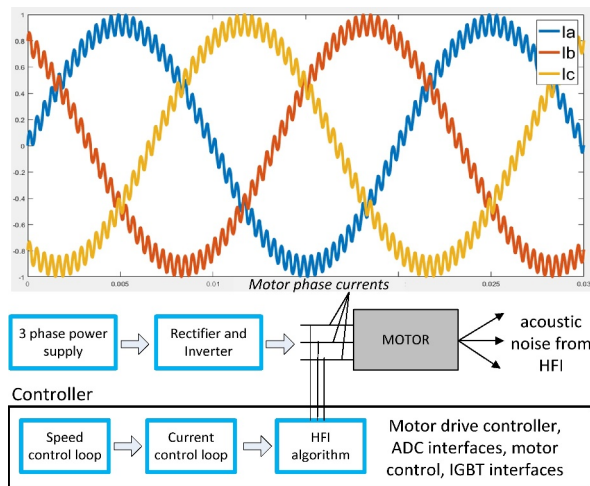


FIGURE 3 High frequency Injection for a 3-phase motor.

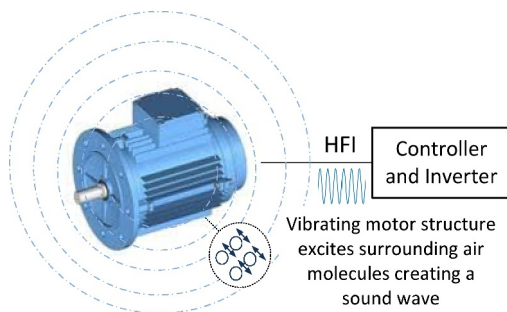


FIGURE 4 High frequency injection active noise control system diagram.

microphone. The motor controller in that case along with managing the spinning of the motor would also process the captured audio and inject anti-phase sound waves using HFI.

4.2 | Merits of the method

The advantages versus a conventional ANC method can be summarised below:

- **Hardware re-use:** the method re-uses the already available torque producing infrastructure of a motor drive to generate sound without the need for installation of speakers. It therefore adds a noise cancellation capability to an otherwise conventional motor drive. The proposed method can be useful, for example, to upgrade the DSP code of an existing motor drive to optimise its acoustics.
- **ANC at the source of the noise:** being able to create anti-noise within the motor's infrastructure can cancel acoustic noise at its source rather than at a distance. An example application taking advantage of this feature is the propeller HFI ANC application presented below.

4.3 | Possible applications of the method

Although this paper attempts to prove the main concept of the proposed HFI ANC method, the ANC approach can be expanded into a number of example applications presented below and shown diagrammatically in Figure 5:

- **Propeller Noise** (Figure 5a): propeller noise is of special interest as it is an upcoming hurdle for electric/hybrid aircraft propulsion and a known problem in submarine propulsion. Research efforts [40] and commercial products by Ultra [3] are two existing examples of aircraft propeller ANC while ref. [5] is an example of submarine propeller ANC. However, the above methods involve the use of speakers to create anti-noise rather than the proposed application of HFI. It is worth noting that the noise generated from a propeller has both tonal and wideband noise frequency elements due to phenomena named thickness and loading noise [41, 42]. With tonal noise being a dominant part of propeller noise [42], the experiments in Section 5 of this paper focus on tonal noise cancellation.
- **Pair of sensorless motor drives** (Figure 5b): the HFI ANC method may have in some applications dual function. Firstly, towards conventional sensorless position calculation and secondly, for noise cancellation purposes. Under this example of applications, HFI is used by two sensorless motor drives and their injection voltage is of the same frequency but of anti-phase relation resulting in the acoustic noise of each motor drive, cancelling each other without the need of a microphone.
- **ANC of external subsystem** (Figure 5c): under this example, the acoustic noise to be cancelled by the method originates from an external source. For example, it may be

known that an external subsystem will pollute the system with a tonal or wideband noise, and therefore, HFI is applied to create anti-noise.

5 | EXPERIMENTAL RESULTS ON THE HEMAS PLATFORM

5.1 | The HEMAS drive

The rotor of a helicopter and specifically the rotation of the rotor blades are used to establish the necessary lift for the helicopter to become airborne [43]. In order to control the direction, altitude, and speed of flying, the angle of the rotor blades needs to be adjusted. The pilot is able to control the angle of the blades using a device known as swashplate. The swashplate is situated below the rotor blades as shown in Figure 6 and can change the angle of the blades individually or collectively as they revolve. Primary control systems including the swashplate have been in the past decades controlled using hydraulics. In alignment with the more electric aircraft (MEA) initiative, the HEMAS was developed to control the swashplate using a set of PMSMs [43]. The HEMAS actuation system was

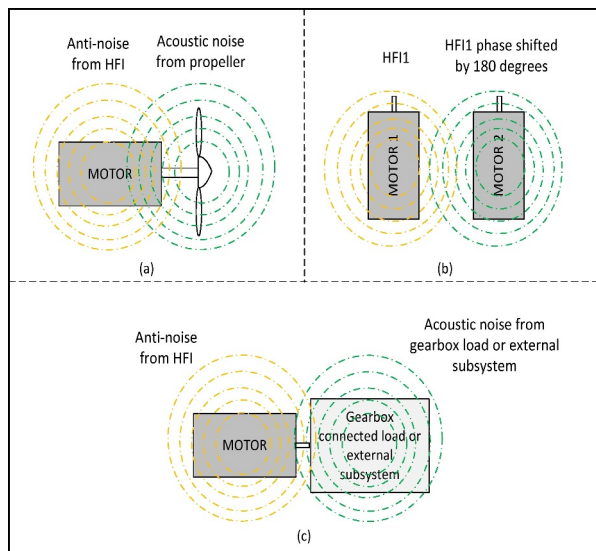


FIGURE 5 Example applications of the high frequency injection active noise control method, (a) propeller noise, (b) pair of sensorless motor drives, (c) ANC of external subsystem.

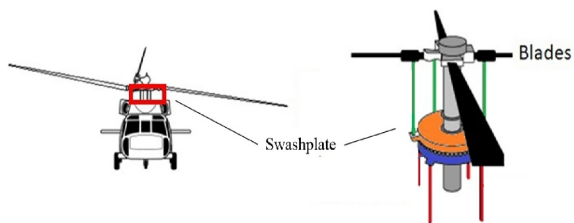


FIGURE 6 Helicopter swash plate.

developed more than a decade ago as part of the European Clean Sky JTI Research Programme in collaboration between EADS-IW, Eurocopter, Liebherr-Aerospace, and Agusta Westland. The research presented in this paper uses the HEMAS test rig illustrated in Figure 7 to demonstrate the HFI ANC method. The parameters of the HEMAS electrical machine are listed in Table 1 [43].

5.2 | Experimental setup

Aiming to analyse the relationship between HFI and acoustics, the test set up is based on the storage and analysis of two types of data, DSP and Acoustic Data (see Figure 8). DSP data involves a 1000-element array internal to the DSP registers storing HFI voltage, motor phase currents, and rotor angle. DSP data is sampled at the Pulse Width Modulation (PWM) frequency of 10 kHz. Acoustic data is produced by the capturing of the acoustic noise using a microphone at a sampling rate of 48 kHz and 256 kbps quality. Both types of data are imported in Matlab for analytical purposes. This side-to-side analysis of DSP and audio data provides clarity on the correlation between HFI and acoustics investigated in this paper. Note that a microphone was used instead of a sound



FIGURE 7 The helicopter electro-mechanical actuation system test rig.

TABLE 1 HEMAS Motor parameters.

Parameter description	Notation	Value
No. of pole pairs	p	5
Maximum speed	n_{\max}	5200 [rpm]
Rated current	I_n	4.7 [A]
Peak current	I_{\max}	34 [A]
Peak power	P_{\max}	2.6 [kW]
Efficiency	η_m	98.8 [%]
Phase resistance	R_S	0.23 [Ω]
Phase inductance	L	1.193 [mH]
Voltage constant	κ_E	0.092 [V/rads]
Torque constant	κ_T	0.142 [Nm/A]

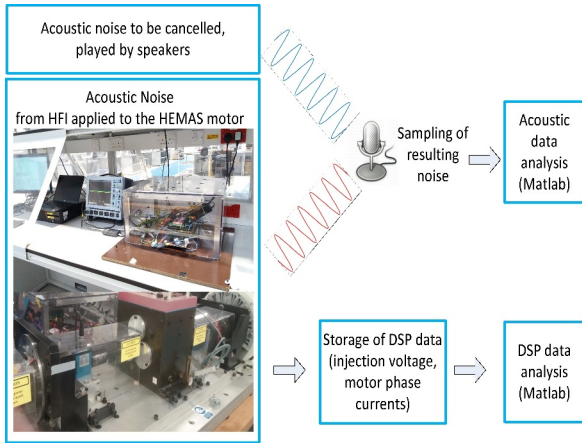


FIGURE 8 Helicopter electro-mechanical actuation system high frequency injection active noise control test set up.

level metre as it was found useful to perform analysis in the time and frequency domain of the resulting sound waves. In future testing, the use of a sound level metre is also planned to be included.

5.3 | Sound waves from HFI

The first experiment performed on the HEMAS platform intends to characterise the acoustic noise that originates from HFI and compare these findings with the theoretical analysis of Section 2.2. In this experiment, 1.4, 1.5, 1.7, and 2 kHz HFI voltage is applied to the HEMAS motor as per Figures 9–12. For simplicity, equal HF voltage is applied to both d and q axis. Figures 9a–12a illustrate the injection voltage to the d/q axis and Figures 9b,c–12b,c display the resultant HF currents on the synchronous frames. Figures 9d–12d display the FFT of the injection voltage, and Figures 9e–12e display the FFT of resultant currents. Finally, Figures 9f–12f show the acoustic noise from HFI.

From Figures 9a,d–12a,d, it can be seen that HF voltage of n kHz (where $n = 1.4, 1.5, 1.7, 3$) results in the HF current of the same frequency along with lower amplitude harmonics. As torque is proportional to current and the vibration of the motor at n kHz excites the surrounding air molecules, the frequency of the generated acoustic noise (Figures 9f–12f) is also centred at n kHz along with lower amplitude harmonics. These acoustic harmonics exist for a number of reasons, namely the selected PWM switching frequency, device non-linearities, and the acoustic sampling process. As the PWM switching frequency of 10 kHz is close to the HF injection frequency, the voltage demand steps cannot construct a perfect sinusoid, and the resultant currents are non-sinusoidal appearing as harmonics. In a similar manner, the current becomes distorted due to inverter non-linearities. Finally, the sampled audio goes through a further small distortion process during the digitisation process by the microphone and Analogue-to-Digital Converter. Observing the FFT shape of Figures 9d,e–12d,e, there appears to exist some frequency

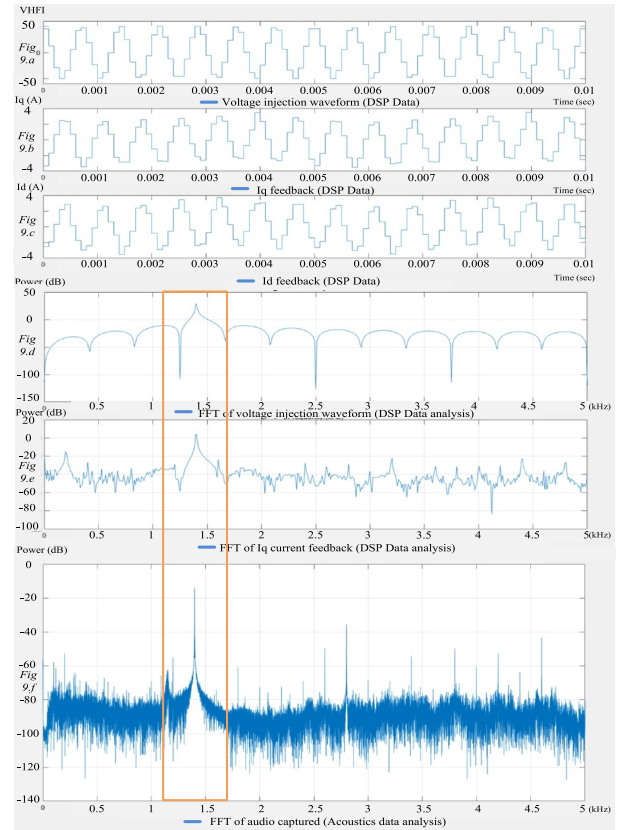


FIGURE 9 Digital signal processing logged data and acoustics from high frequency injection 1.4 kHz.

leakage. This visual artefact is primarily related to the limitation on the number of data samples within the DSP. Analysing the overall results from Figures 9–12, one conclusion that can be made is by controlling the injection frequency of HFI; it is possible to control the frequency of the acoustic noise, therefore validating the analysis of Section 2.2.

5.4 | ANC by means of HFI

Having validated the relationship between HFI and acoustics, it is now possible to harvest these findings and use the sound-waves from HFI towards ANC. To illustrate the effectiveness of the proposed method, this experiment is conducted by contaminating the system with a tonal noise from speakers. The acoustic noise from HFI is then used to perform ANC while monitoring the resultant acoustic noise using a microphone. The set up for this experiment is shown in Figure 8. A Matlab-generated sinusoidal waveform of frequency f_{speaker} is therefore played back using a speaker at close proximity to the HEMAS rig, and HFI is enabled at frequency f_{HFI} to initiate ANC and cancel the speaker noise. The desired relation of the two waveforms for the noise cancellation to take place is $f_{\text{speaker}} = f_{\text{HFI}}$ and the two waveforms to be in anti-phase (180° phase offset to each other). Aiming to illustrate how the noise and anti-noise waveforms interact in the air, a more intuitive

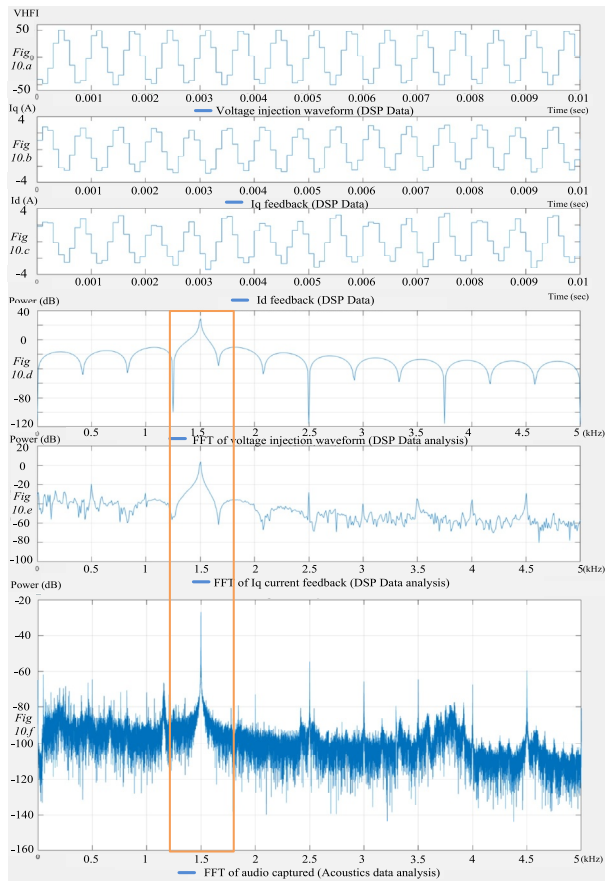


FIGURE 10 Digital signal processing logged data and acoustics from high frequency injection 1.5 kHz.

approach is followed. The two frequencies f_{speaker} and f_{HFI} are slightly different from each other by such a degree that one waveform naturally slides versus the other within a predefined amount of time. This approach is also beneficial as the relation between noise and anti-noise in an equal frequency test may not hold, therefore introducing inaccuracies of the optimal noise cancellation that can be achieved. Specifically, if $f_{\text{speaker}} = 1499.9$ Hz and $f_{\text{HFI}} = 1500.0$ Hz, then the two waveforms are in anti-phase relationship once every 10 s while for the rest of the time they slowly slide against each other. Similarly, if $f_{\text{speaker}} = 1499.8$ Hz and $f_{\text{HFI}} = 1500.0$ Hz, this sliding behaviour takes place once every 5 s. The full list of frequency pairs (f_{speaker} and f_{HFI}) to be tested in this experiment is presented in Table 2. Preliminary visual sound propagation analysis was performed using Matlab's k -Wave as shown in Figure 13. A simple Matlab simulation illustrating the sliding behaviour for each of the frequency pairs was then performed and is shown in Figures 14–21. Following this analysis, the experiment was conducted for each of the selected frequency pairs of Table 2. The experiment was conducted firstly by enabling only the motor's HFI, followed by only the speaker tonal noise, and finally both noise sources (speaker and HFI) allowing the ANC process to take place as shown in Figures 22–29. This sequence was adopted so as to calibrate the amplitude of the two acoustic waveforms.

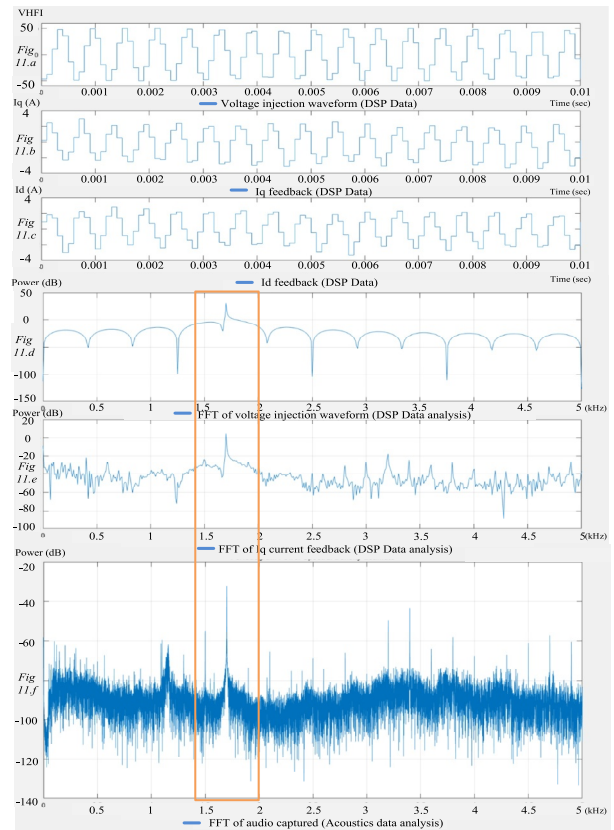


FIGURE 11 Digital signal processing logged data and acoustics from high frequency injection 1.7 kHz.

The first observation from Figures 22–29 is that the resultant noise increases and decreases over time as per Matlab simulations shown in Figures 14–21, therefore, confirming that the noise cancellation is taking place. Note that although it might appear at first sight that the resultant noise at certain points is higher than the original noise to be suppressed, the point in time-of-interest used in analysis is when the two sound waves are in anti-phase that results in maximum noise reduction.

The noise improvement from each HFI ANC test is summarised in Table 3 and is shown diagrammatically for one test in Figure 30. Note that a varying degree of acoustic noise reduction is observed ranging between 39% and 68%. This variation is primarily because the tuning of the amplitude of the two waveforms (HFI/speaker) was manual. If the two waveforms were matched in an automated manner, the cancellation process would be more effective and results would improve considerably.

The physical acoustic observation of a human witnessing the above experiment is that every few seconds the noise increases and decreases over time in a periodic manner. One of the audio captures is provided to the reader for the physical evaluation of the method from the frequency pair of 1699.8 Hz/1700 Hz shown in Figure 27. The audio sample is located at <https://youtu.be/35lnaj2w33Q>. One key difference between simulations shown in Figures 14–21 and hardware

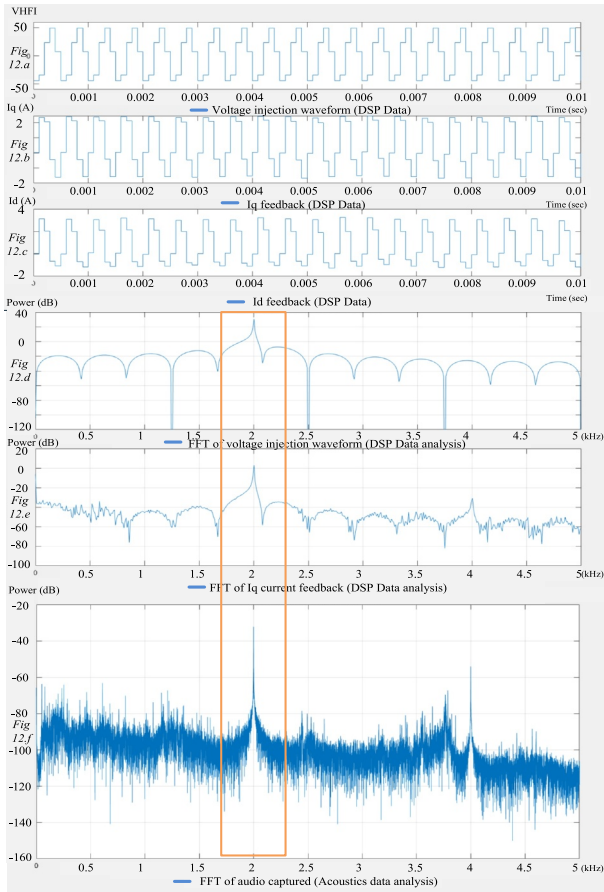


FIGURE 12 Digital signal processing logged data and acoustics from high frequency injection 2 kHz.

TABLE 2 HFI ANC sliding frequency test table.

$f_{\text{speaker}}(\text{Hz})$	$f_{\text{HFI}}(\text{Hz})$	ANC period
1399.9	1400	10 s
1399.8	1400	5 s
1499.9	1500	10 s
1499.8	1500	5 s
1699.9	1700	10 s
1699.8	1700	5 s
1999.9	2000	10 s
1999.8	2000	5 s

testing shown in Figures 22–29 is that the resultant acoustic noise does not attenuate completely down to 0. This is firstly because there is some ambient environmental noise within the lab and secondly because HFI produces some low amplitude harmonics. However, despite this harmonic generation, the overall noise is reduced. The effectiveness of the method can be improved by reducing these harmonics if the PWM frequency was to be increased from the current setting of 10 kHz.

Analysing the acoustic levels of noise and anti-noise, it can be observed that the sound amplitude levels do not match that

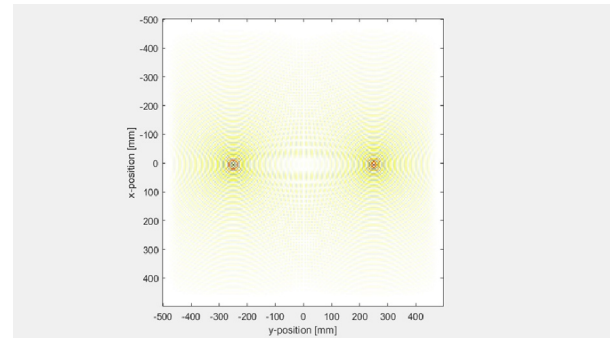


FIGURE 13 Analysis of sound propagation in Matlab's *k*-wave.

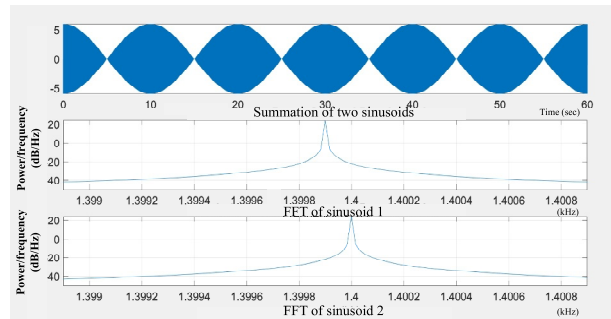


FIGURE 14 Summation simulation 1399.9 Hz 1400 Hz.

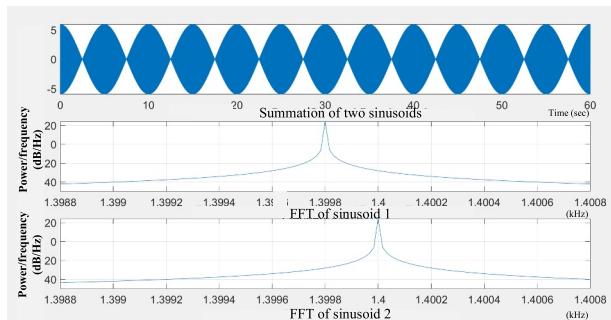


FIGURE 15 Summation simulation 1399.8 Hz 1400 Hz.

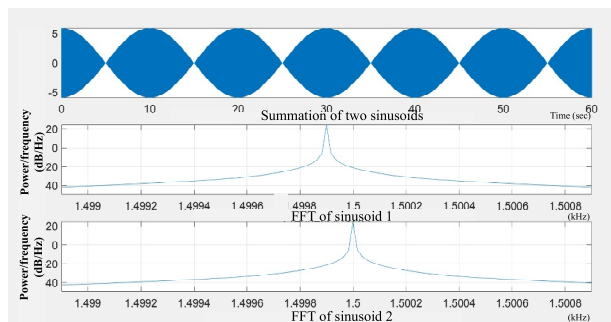


FIGURE 16 Summation simulation 1499.9 Hz 1500 Hz.

of an aircraft. Additionally, the test method is performed in open-loop manner rather than synchronising to an incoming audio signal. If the method was to be applied in a product, the

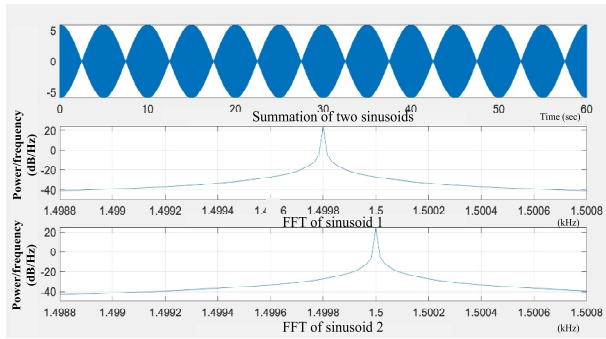


FIGURE 17 Summation simulation 1499.8 Hz 1500 Hz.

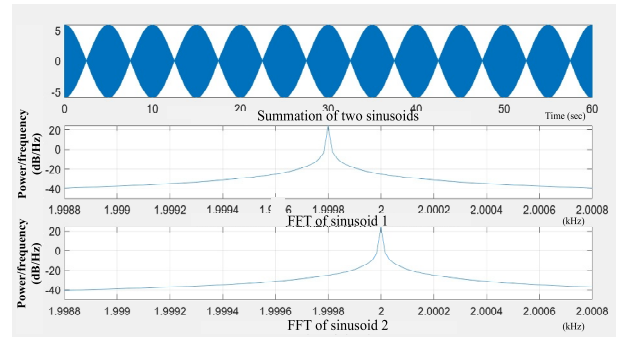


FIGURE 21 Summation simulation 1999.8 Hz 2000 Hz.

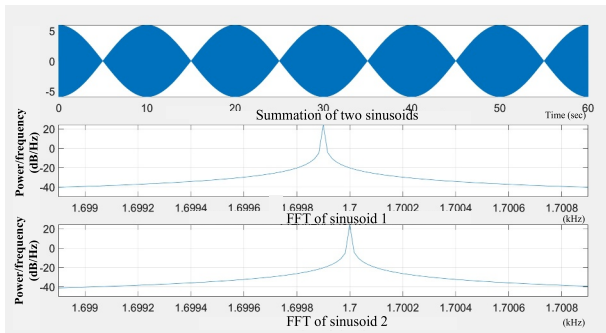


FIGURE 18 Summation simulation 1699.9 Hz 1700 Hz.

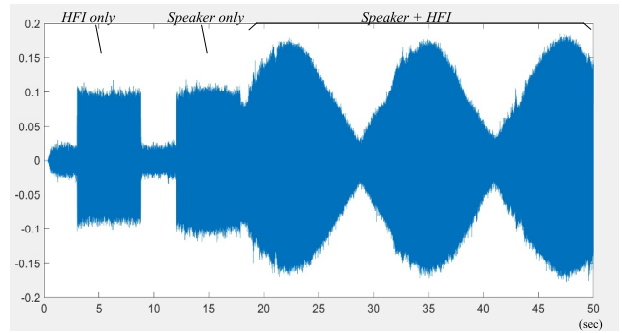


FIGURE 22 Active noise control helicopter electro-mechanical actuation system, $f_{\text{speaker}} = 1399.9$ Hz $f_{\text{HFI}} = 1400$ Hz.

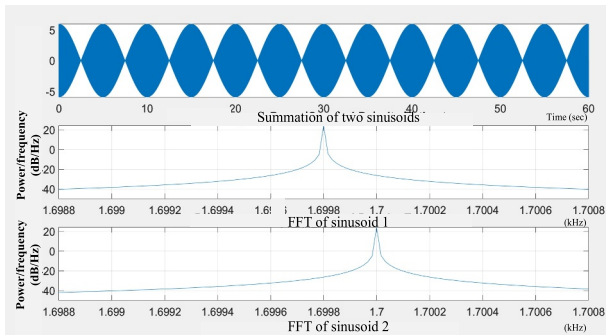


FIGURE 19 Summation simulation 1699.8 Hz 1700 Hz.

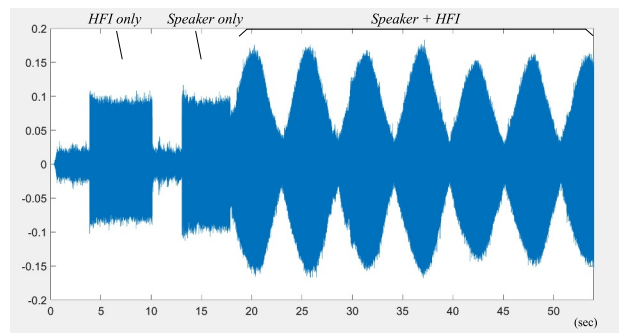


FIGURE 23 Active noise control helicopter electro-mechanical actuation system, $f_{\text{speaker}} = 1399.8$ Hz $f_{\text{HFI}} = 1400$ Hz.

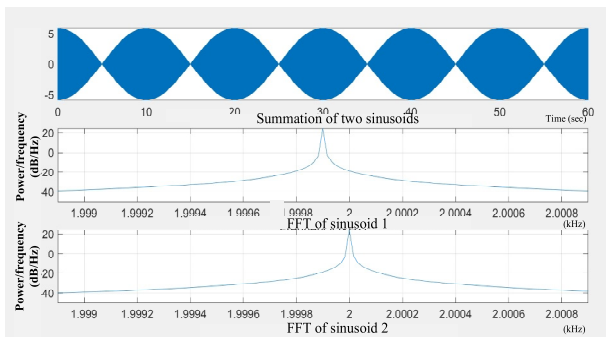


FIGURE 20 Summation simulation 1999.9 Hz 2000 Hz.

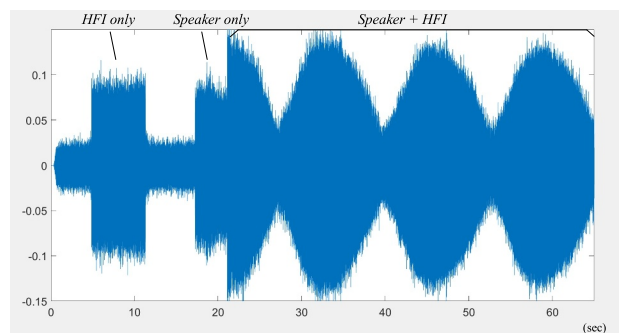


FIGURE 24 Active noise control helicopter electro-mechanical actuation system, $f_{\text{speaker}} = 1499.9$ Hz $f_{\text{HFI}} = 1500$ Hz.

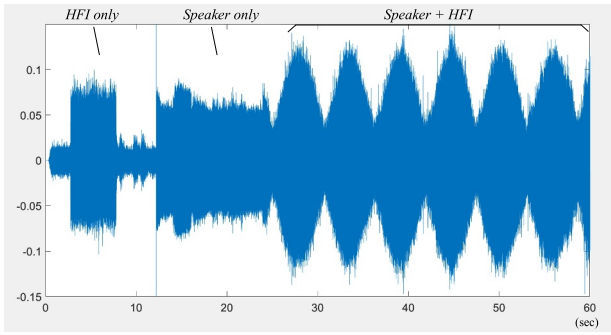


FIGURE 25 Active noise control helicopter electro-mechanical actuation system, $f_{\text{speaker}} = 1499.8 \text{ Hz}$ $f_{\text{HFI}} = 1500 \text{ Hz}$.

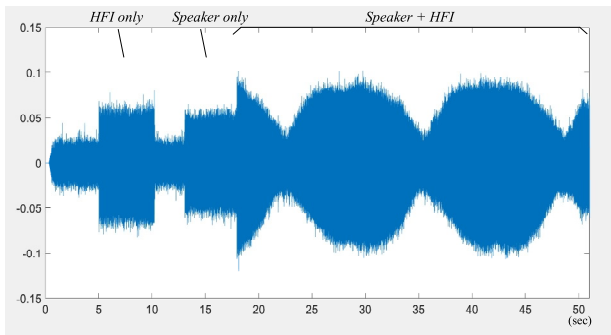


FIGURE 26 Active noise control helicopter electro-mechanical actuation system, $f_{\text{speaker}} = 1699.9 \text{ Hz}$ $f_{\text{HFI}} = 1700 \text{ Hz}$.

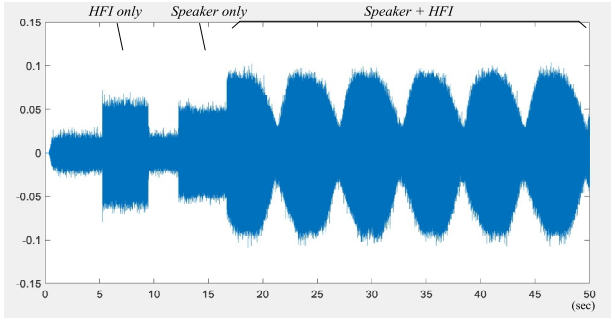


FIGURE 27 Active noise control helicopter electro-mechanical actuation system, $f_{\text{speaker}} = 1699.8 \text{ Hz}$ $f_{\text{HFI}} = 1700 \text{ Hz}$.

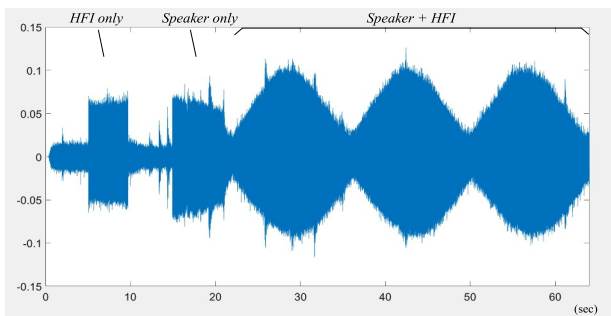


FIGURE 28 Active noise control helicopter electro-mechanical actuation system, $f_{\text{speaker}} = 1999.9 \text{ Hz}$ $f_{\text{HFI}} = 2000 \text{ Hz}$.

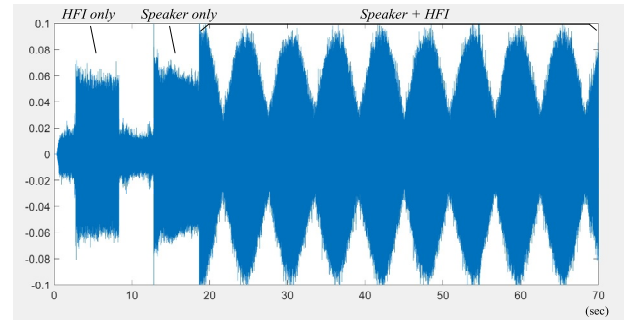


FIGURE 29 Active noise control helicopter electro-mechanical actuation system, $f_{\text{speaker}} = 1999.8 \text{ Hz}$ $f_{\text{HFI}} = 2000 \text{ Hz}$.

TABLE 3 HFI ANC Noise reduction analysis.

Test frequency pair	Noise reduction using the HFI ANC method
1399.9/1400 Hz	68%
1399.8/1400 Hz	61%
1499.9/1500 Hz	53%
1499.8/1500 Hz	39%
1699.9/1700 Hz	52%
1699.8/1700 Hz	44%
1999.9/2000 Hz	60%
1999.8/2000 Hz	56%

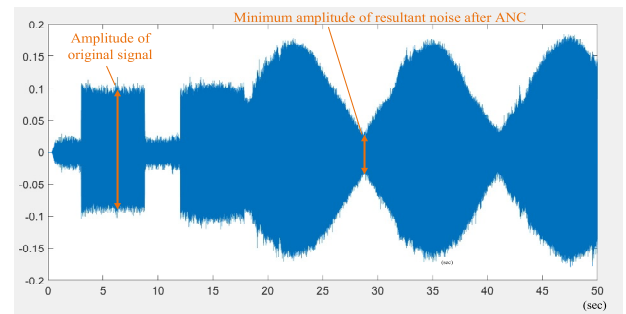


FIGURE 30 Helicopter electro-mechanical actuation system testing active noise control gain illustration.

method would function in a closed-loop manner. The controller would process the sampled audio noise to be suppressed and calculate not only the frequency but also the phase of the anti-noise taking into account propagation delays. The purpose of the experiment however, was to illustrate the concept of HFI ANC and not to demonstrate the function of a complete commercial product. The method can be scaled up in terms of amplitude and upgraded to closed-loop functionality to match the expected anti-phase noise characteristics. From the data in Figures 22–29, one additional observation is that the sliding period is slightly higher than the expected 10 s and

5 s of Matlab simulations as shown in Figures 14–21. This additional delay is consistent with the playback laptop and the HEMAS hardware being relatively misaligned on measuring time by an error of about 8 ns per sinusoidal cycle. This delay is due to oscillator/Phase Locked Loop drift of the two acoustic systems (HEMAS/laptop). Such a frequency drift is typically encountered on oscillator components upon ageing [44] or upon exposure to temperature variations. However, this frequency deviation would have an exceptionally small impact on the ANC process as 8 ns error over a HFI sinusoidal period of 666,667 ns for the 1.5 kHz experiment is negligible.

5.4.1 | Limitations of the HFI ANC method

Although the proposed method is shown in the above section to achieve ANC, there are some limitations when it is applied to a motor drive application.

The first limitation involves the reduction of the motor's efficiency as a portion of the power consumed is invested on spinning producing torque and a portion is invested on HF vibrations resulting in the generation of acoustic waves.

An additional limitation of HFI methods is HF losses that in turn result in an increase of the motor's temperature [45, 46]. To understand the thermal effects of HFI, it is necessary to first identify the different types of HF losses. Core and copper losses of the windings are the main heat source for PMSM drives [45]. Considering a sinusoidal magnetic field, iron losses can be decomposed to hysteresis, eddy currents, and excess losses as shown in Equation (16):

$$P_{\text{iron}} = P_{\text{hyst}} + P_{\text{eddy}} + P_{\text{exc}} \quad (16)$$

where P_{hyst} , P_{eddy} , P_{exc} are hysteresis, classical eddy, and excess losses, respectively.

Providing a more detailed calculation for each type of losses Equation (16) becomes

$$P_{\text{iron}} = k_{\text{hyst}} f^a B^b + k_{\text{eddy}} f^2 B^2 + k_{\text{exc}} f^2 B^2 \quad (17)$$

where f and B are frequency and peak flux density, k_{hyst} , k_{eddy} , and k_{exc} are constant coefficients, while a and b exponents represent material constants.

HF copper losses are due to the power dissipated to the windings resistance as shown in Equation (18):

$$P_{Cu} = m I_{\text{HF}}^2 R_T \quad (18)$$

where m is the number of motor phases, I_{HF} is the HF current, and R_T is the phase resistance at temperature T .

Core and copper losses are proportional to the amplitude of the HF voltage [46]. Under the proposed HFI ANC method, the higher the amplitude of an acoustic wave needed for acoustic purposes, the higher the resultant losses and temperature induced to the motor drive. As a result of this limitation, additional thermal analysis and some temperature

monitoring needs to be put in place to compensate for this shortcoming.

Additionally, upon high loading conditions, the available power and DC Link voltage as well as the motor's temperature may necessitate the power invested on acoustics to be reduced so as to accommodate the speed, voltage demands, and thermal limitations of the motor drive. A management scheme is therefore needed to limit the power consumption of the acoustic generation function and prioritise power invested on spinning when needed.

Despite the above limitations of the method on efficiency, system losses, and thermal performance, there are certain applications where the gains of the HFI ANC method outweigh its drawbacks. For instance, when an aircraft is landing or taking off in a residential area, it can enter an increased acoustic suppression mode to comply with regulations and improve the quality-of-life for nearby residents. Similarly, these limitations can be acceptable if the method is applied to reduce the acoustic signature of a submarine or of a military vessel.

5.5 | Acoustic versatility evaluation

Section 5.4 showed that the HFI ANC method can be used towards reducing the acoustic noise within a system. However, one possible question that could be posed is whether a motor drive is versatile enough to generate acoustic waves. Aiming to demonstrate the acoustic flexibility of the method in a creative manner, HFI is set up so that the HEMAS platform acts as a musical instrument. A sequence of musical notes from a recognisable classical masterpiece, namely “Eine Kleine Nachtmusik” by Mozart, is produced by means of HFI. The implementation code of the motor's digital controller was therefore updated with an array of HFI notes and durations so as to synthesise the selected classical song.

The acoustic capture of the song produced by HFI applied to the HEMAS drive can be listened by following the link given below: HFI E. Kleine Octave4:

<https://youtu.be/Y2mP2A0oCtA>

Listening to the song produced by the HEMAS drive and taking into consideration that the machine was never designed to produce acoustic waves, it is of significant interest appreciating the acoustic capabilities over a range of frequencies.

6 | CONCLUSION

This paper has presented the method of Acoustic Noise Control using HF injection. The HFI ANC process uses the existing electrical and mechanical infrastructure of a motor drive to cancel existing noise residing within the system. It presented the theoretical framework of the method, followed by analysis and experimental testing on the HEMAS. The results shown in Section 5.3 illustrated that it is possible to control the frequency of the generated acoustic noise by

controlling the frequency of the HFI. Section 5.4 showed that acoustic improvements can be obtained from the proposed ANC method, reducing tonal noise 39%–68%. This improvement is considered substantial taking into consideration that the PWM switching frequency is set to 10 kHz, and the digital/analog technology used is more than a decade old. Additionally, the method could be expanded to cancel wide-band noise using a closed loop approach. The results shown in Section 5.5 illustrated the versatility of the method producing sound waves over a wide range of musical frequencies. Considering the increased levels of electrification in the aerospace, land, and marine sectors [47], the proposed method could have a significant impact on the acoustics of systems deploying motor drives.

AUTHOR CONTRIBUTION

Stefanos Skoulaxinos: Conceptualisation; data curation; formal analysis; investigation; methodology; validation; visualisation; writing – original draft; writing – review & editing. **Pat Wheeler:** Conceptualisation; funding acquisition; supervision; writing – review & editing. **Gaurang Vakil:** Conceptualisation; funding acquisition; supervision; writing – review & editing.

ACKNOWLEDGEMENTS

This project has, in part, been funded by the Clean Sky 2 Joint Undertaking under the European Union's Horizon 2020 research and innovation programme under grant agreement 831877. S. Skoulaxinos thanks his supervisors at the PEMC Group for their valuable guidance and support throughout this research effort. S. Skoulaxinos also thanks his employer Collins Aerospace (Raytheon Technologies) for covering the tuition fees for this Part Time research at the PEMC group of Nottingham University.

CONFLICT OF INTEREST STATEMENT

The authors declare that there is no conflict of interest.

DATA AVAILABILITY STATEMENT

The data that supports the findings of this study is available from the corresponding author upon reasonable request.

ORCID

Stefanos Skoulaxinos  <https://orcid.org/0000-0001-5001-1224>

REFERENCES

- ANC Patent by Paul Lueg Process of silencing sound oscillations. <https://patents.google.com/patent/US2043416>
- ANC patent by Lawrence J Fogel: Apparatus for improving intelligence under high ambient noise levels. <https://patents.google.com/patent/US2966549A/en>
- Hinchliffe, R., et al.: Tonal active control in production on a large turbo-prop aircraft. In: INTER-NOISE and NOISE-CON Congress and Conference Proceedings, pp. 369–376 (2002)
- Ultra ANC system delivery news. <https://www.aviationtoday.com/2009/04/20/ultra-delivers-1000th-anc-system/>
- Howard, C.: Recent developments in submarine vibration isolation and noise control. In: Proceedings of 1st Submarine Science Technology and Engineering Conference, Adelaide, SA, Australia (2011)
- University of Sheffield, reference to BAE systems centre for research in active control (CRAC). [Online]. <https://www.southampton.ac.uk/people/5x7sy9/professor-stephen-daley>
- Li, X., et al.: Feasibility of active vibration isolation of diesel engines in Collins class submarines. *Nav. Eng. Bulletin.*, 25–26 (2004)
- Von Drathen, A.: Propulsion System Solutions for Present and Future Naval Vessels, pp. 27–29. Pacific 2010, Sydney (2010)
- Moon, S.-J., et al.: A study on the hybrid mount against vibration and shock for naval ships. *Shock Vib.* 17(3), 269–283 (2010). <https://doi.org/10.3233/SAV-2010-0511>
- Choi, S.-B., et al.: A piezostack-based active mount for broadband frequency vibration control: experimental validation. *Smart Mater. Struct.* 18(9), 097001 (2009). <https://doi.org/10.1088/0964-1726/18/9/097001>
- Gertsen and Olufsen: G&O vibration compensator. [Online] http://www.g-o.dk/Ship_-_Offshore/Products/G-O_Brands/G-O_Vibration_Compensator.aspx. Accessed 8 October 2011
- Silentium website: <https://www.silentium.com/automotive-2/>
- Bafti, P.S., et al.: Active noise suppression of SISO model using a filtered X-LMS algorithm. In: 2009 International Conference on Signal Acquisition and Processing, pp. 39–42. IEEE (2009)
- Qiu, X., Hansen, C.H.: A modified filtered-x LMS algorithm for active control of periodic noise with on-line cancellation path modelling. *J. Low Freq. Noise Vib. Act. Control* 19(1), 35–46 (2000). <https://doi.org/10.1260/0263092001492787>
- Troshin, A.G., SangGon, C., DongHwan, K.: Evaluation and parametric study of LMS algorithms family for active noise control barriers. In: International Conference on Control, Automation and Systems (ICCAS 2011), pp. 1656–1659. IEEE (2011)
- Jang, H., et al.: KTX's interior noise reduction performance comparison for each section using multichannel active noise control. In: 2012 12th International Conference on Control, Automation and Systems. IEEE (2012)
- Jiang, H.: Audible Noise Reduction in the High Frequency Injection Based Sensorless Torque Control for EPS Applications. Ph.D thesis, pp. 55–79. University of Nottingham (2012). ch 3
- Wang, G., Zhang, G., Xu, D.: Position Sensorless Control Techniques for Permanent Magnet Synchronous Machine Drives, 1st ed, pp. 81–88. Springer (2019). ch. 4
- Bojoi, R., et al.: Sensorless control of PM motor drives — a technology status review. In: IEEE Workshop on Electrical Machines Design, Control and Diagnosis (WEMDCD), 2013, pp. 168–182. IEEE (2013)
- Alaei, A., et al.: Dynamic performance analysis of high frequency signal injection based sensorless methods for IPM synchronous motors. In: IEEE 9th Annual Power Electronics, Drives Systems and Technologies Conference (PEDSTC), pp. 151–156. IEEE (2018)
- Ghazimoghadam, M.A., Tahami, F.: Sensorless control of non-salient PMSM using asymmetric alternating carrier injection. In: IEEE Symposium on Industrial Electronics and Applications, pp. 7–12. IEEE (2011)
- Ahmed, S.M., Lefley, P.W.: A new simplified sensorless control method for a single phase SR motor using HF signal injection. In: IEEE 42nd International Universities Power Engineering Conference, pp. 1075–1078. IEEE (2007)
- Siu, M.K.L., Woo, K.T.: A high-frequency signal injection based sensorless drive method for brushless DC motor. In: IEEE 18th International Conference on Advanced Robotics (ICAR), pp. 367–372. IEEE (2017)
- Wang, D., et al.: A hybrid speed sensorless control of induction machine based on adaptive flux observer and high-frequency signal injection method. In: IEEE 19th Workshop on Control and Modeling for Power Electronics (COMPEL), pp. 1–5. IEEE (2018)
- Liu, J.M., Zhu, Z.Q.: Sensorless control strategy by square-waveform high-frequency pulsating signal injection into stationary reference frame. *IEEE J. Emerg. Sel. Top. Power Electron.* 2(2), 171–180 (2014). <https://doi.org/10.1109/jestpe.2013.2295395>
- Benjak, O., Gerling, D.: Review of position estimation methods for PMSM drives without a position sensor, part III: methods based on saliency and signal injection. In: IEEE International Conference on Electrical Machines and Systems, pp. 873–878. IEEE (2010)

27. Medjmadj, S., et al.: PMSM drive position estimation: contribution to the high frequency injection voltage selection issue. *IEEE Trans. Energy Convers.* 30(1), 349–358 (2015). <https://doi.org/10.1109/tec.2014.2354075>
28. Sabine, P.E.: *Acoustics and Architecture*, pp. 1–11. McGraw-Hill Book Company Inc (1932). ch. 1
29. Wellman, M.E.: RANS-based Mixing Noise Predictions of Installed Asymmetric Jet Flows. Ph.D thesis. University of Southampton (2023)
30. Salomons, E.M., Lohman, W.J.A., Zhou, H.: Simulation of sound waves using the lattice Boltzmann method for fluid flow: benchmark cases for outdoor sound propagation. *PLoS One* 11(1), e0147206 (2016). <https://doi.org/10.1371/journal.pone.0147206>
31. Chevaugnon, N., et al.: Efficient discontinuous galerkin methods for solving acoustic problems. In: 11th AIAA/CEAS Aeroacoustics Conference, 23–25 May 2005, Monterey, CA, USA, AIAA, pp. 2005–2823 (2005)
32. Agarwal, A., Morris, P.J., Mani, R.: Calculation of sound propagation in nonuniform flows: suppression of instability waves. *AIAA J.* 42(1), 80–88 (2004). <https://doi.org/10.2514/1.619>
33. Self, R.H., Bassetti, A.: A RANS based jet noise prediction scheme. In: 9th AIAA/CEAS Aeroacoustics Conference and Exhibit, Hilton Head, South Carolina, May 2003 AIAA 2003-3325, pp. 3325 (2003)
34. Attenborough, K.: *Sound Propagation in the Atmosphere*. Springer Handbook of Acoustics (2014). Chapter 4
35. Chen, H.: *Theory and Design of Spatial Active Noise Control Systems*. Ph.D Thesis. Australian National University (2017)
36. Wilson, K., Pettit, C.L., Ostashev, V.E.: Sound propagation in the atmospheric boundary layer. *Acoust. Today, Sprin* 11(2) (2015)
37. Bass, H.E., Sutherland, L.C., Zuckewar, A.J.: Atmospheric absorption of sound: further developments. *J. Acoust. Soc. Am.* 97, 680–683 (1995)
38. Schissler, C.: *Efficient Interactive Sound Propagation in Dynamic Environments*. Ph.D thesis at the University of North Carolina at Chapel Hill (2017)
39. Kamman, J.W., Naghshineh, K.: A comparison of open-loop feedforward and closed-loop methods for active noise control using volume velocity minimization. *Appl. Acoust.* 57(1), 29–37 (1999). [https://doi.org/10.1016/s0003-682x\(98\)00043-7](https://doi.org/10.1016/s0003-682x(98)00043-7)
40. Johansson, S., et al.: Evaluation of multiple reference active noise control algorithms on Dornier 328 aircraft data. *IEEE Trans. Speech Audio Process.* 7(4), 473–477 (1999). <https://doi.org/10.1109/89.771319>
41. Astley, R.J.: *Predicting and Reducing Aircraft Noise*. ICSV14, 14th International Congress on Sound Vibration, Cairns, Australia (2007)
42. Haddaoui, M.: *Development of a Propeller Source Noise Model*. MSc thesis, pp. 3–14. Delft University of Technology (2019). ch. 2
43. Rottach, M.: *Drive-System Optimization for a Helicopter Electromechanical Actuation System*. Ph.D Thesis, pp. 8–35. University of Nottingham (2014). ch. 2
44. Mizan, M.: *Ceramic dielectric resonator oscillator aging*. In: *IEEE Proceedings 48th Annual Symposium on Frequency Control*, pp. 466–471 (1994)
45. Zhao, J., Wu, X.: *Thermal analysis of permanent Magnet synchronous motor based on equivalent thermal network method*. In: *2022 25th International Conference on Electrical Machines and Systems (ICEMS)*, pp. 1–4. IEEE (2022)
46. Alaci, A., et al.: *Reduction of high-frequency injection losses, acoustic noise and total harmonic distortion in IPMSM sensorless drives*. *IET Power Electron.* 12(12), 3197–3207 (2019). <https://doi.org/10.1049/iet-pel.2018.6250>
47. Valente, G., et al.: *Design methodology and parametric design study of the on-board electrical power system for hybrid electric aircraft propulsion*. In: *IET 10th International Conference on Power Electronics, Machines and Drives (PEMD)*, pp. 448–454 (2020)

How to cite this article: Skoulaxinos, S., Wheeler, P., Vakil, G.: Active noise control by means of high frequency injection in electric motors. *IET Electr. Power Appl.* 1–15 (2024). <https://doi.org/10.1049/elp2.12442>